VI. Conclusions

In this work, a multiscale textual image compression (TIC) method is introduced. The document image is first decomposed into subimages using a binary subband decomposition structure. Next, the locations of the character images in the subband domain are encoded. In this way, higher compression ratios than regular TIC methods can be obtained without introducing any visual degradation.

Performance of various subband decomposition structures are experimentally tested, and it is observed that the binary wavelet transform and the binary nonlinear subband decomposition structures produce comparable coding results.

A feature of the coding method is that the keyword search or the creation of the symbol library can be carried out in the coded bitstream in subbands. Other advantages of the subband scheme include multiresolution image viewing and computational efficiency. As a direct consequence of the subband decomposition, a low-resolution image x_{ll} is obtained and it can be used for fast preview purposes to decrease the bandwidth usage. The compression of the textual image is a computationally costly operation. The multiresolution approach reduces the encoding time as the pattern matching is carried out in low-resolution images.

References

[1] V. K. Govindan and A. P. Shivaprasad, "Character recognition—A review," *Pattern Recognit.*, vol. 23, pp. 671–683, 1990.

[2] R. N. Ascher and G. Nagy, "A means for achieving a high degree of compaction on scan-digitized printed text," *IEEE Trans. Comput.*, vol. C-23, pp. 1174–1179, Nov. 1974.

[3] W. K. Pratt *et al.*, "Combined symbol matching facsimile data compression system," *Proc. IEEE*, vol. 68, pp. 786–796, July 1980.

[4] M. J. J. Holt, "A fast binary template matching algorithm for document image data compression," in *Pattern Recognit.*, J. Kittler, Ed. Berlin, Germany: Springer-Verlag, 1988.

[5] O. Johnsen, J. Segen, and G. L. Cash, "Coding of two-level pictures by pattern matching and substitution," *Bell Syst. Tech. J.*, vol. 62, pp. 2513–2545, May 1983.

[6] I. H. Witten *et al.*, "Textual image compression: Two-stage lossy/lossless encoding of textual images," *Proc. IEEE*, vol. 82, pp. 878–888, June 1994.

[7] I. H. Witten, A. Moffat, and T. C. Bell, *Managing Gigabytes.* San Mateo, CA: Morgan Kaufmann, 1999.

[8] J. W. Woods, Ed., *Subband Image Coding.* Boston, MA: Kluwer, 1991.

[9] J. M. Shapiro, "Embedded image coding using zerotrees of wavelet coefficients," *IEEE Trans. Signal Processing*, vol. 41, pp. 3445–3462, Dec. 1993.

[10] G. Caire, L. Grossman, and H. V. Poor, "Wavelet transforms associated with finite cyclic groups," *IEEE Trans. Inform. Theory*, vol. 39, pp. 1157–1166, July 1993.

[11] M. D. Swanson and A. H. Tewfik, "A binary wavelet decomposition of binary images," *IEEE Trans. Image Processing*, vol. 5, pp. 1637–1651, Dec. 1996.

[12] F. J. Hampson and J. C. Pesquet, "A nonlinear subband decomposition with perfect reconstruction," in *IEEE Int. Symp. Image Processing*, 1996.

[13] O. Egger, W. Li, and M. Kunt, "High compression image coding using an adaptive morphological subband decomposition," *Proc. IEEE*, vol. 83, pp. 272–287, Feb. 1995.

[14] O. N. Gerek, M. N. Gürcan, and A. E. Çetin, "Binary morphological subband decomposition for image coding," in *IEEE Int. Symp. Time-Frequency and Time Scale Analysis*, 1996.

[15] M. N. Gürcan, O. N. Gerek, and A. E. Çetin, "A morphological subband decomposition structure using GF(N) arithmetic," in *Proc. IEEE Int. Conf. Image Processing*, Switzerland, Sept. 1996.

[16] M. D. Swanson, "Issues in image databases: Coding for content-based browsing and retrieval, data hiding, and copyright protection," Ph.D. dissertation proposal, Dept. Elect. Eng., Univ. Minnesota, Minneapolis, MN, June 3, 1996.

[17] M. D. Swanson, S. Hosur, and A. H. Tewfik, "Image coding for content-based retrieval," in *Proc. 1996 SPIE Conf. Visual Communication and Image Processing*, Orlando, FL, 1996, vol. I, pp. 1–12.

[18] T. Kohonen, *Self Organizing Maps.* Berlin, Germany: Springer-Verlag, 1997.

[19] T. Kohonen, J. Hynninen, J. Kangas, and J. Laaksonen, "SOM_PAK: The self-organizing map program package," Tech. Rep. A31, Lab. Comput. Inform. Sci., Helsinki Univ. Technol., Espoo, Finland, 1996.

[20] R. A. Wilkinson, "NIST special database 8: Machine print database," Nat. Inst. Stand. Technol., Adv. Syst. Div., Image Recognit. Grp., Oct. 1, 1992.

[21] D. S. Doermann and S. Yao, "Generating synthetic data for text analysis systems," in *Proc. 4th Symp. Document Analysis and Information Retrieval*, 1995, pp. 449–467.

On Independent Color Space Transformations for the Compression of CMYK Images

Ricardo L. de Queiroz

***Abstract*—Device- and image-independent color space transformations for the compression of CMYK images were studied. A new transformation (to a YYCC color space) was developed and compared to known ones. Several tests were conducted leading to interesting conclusions. Among them, color transformations are not always advantageous over independent compression of CMYK color planes. Another interesting conclusion is that chrominance subsampling is rarely advantageous in this context. Also, it is shown that transformation to YYCC consistently outperforms the transformation to YCbCrK, while being competitive with the image-dependent KLT-based approach.**

I. Introduction

Images for monitor display are commonly stored or transmitted in popular color spaces such as RGB, CIELAB, YUV, YCbCr, etc. [1], [2]. Images to be printed are commonly rendered in a subtractive color space such as CMYK [1], [2]. Sometimes documents contain pictures in other color spaces that are then converted to CMYK for printing. Good color management practice demands color correction for the printing device [3], [4]. We refer to the printing color space as device-dependent-CMYK or simply device-CMYK.

The color correction process not only maps the input gamut to the device's gamut but it also incorporates other factors such as under-color removal (UCR) and tone-reproduction curves (TRC). Those steps are commonly based on a printer model [3], [4] which is empirically derived. CMYK here refers to device-CMYK where the device is known (the dependence on a device is also true for all color spaces derived from CMYK unless a printer-model-based mapping is performed). It is clear that the conversion between color spaces such as CIELAB and device-CMYK is an ill-posed problem, not only because it converts between three and four color bases, but also because it is not a linear process. Thus, invertibility is not guaranteed.

It is often necessary to compress CMYK images for a number of reasons, such as bandwidth or memory reduction. Fig. 1 shows a

Manuscript received February 18, 1998; revised April 12, 1999. The associate editor coordinating the review of this manuscript and approving it for publication was Dr. Thrasyvoulos N. Pappas.

The author is with Xerox Corporation, Webster, NY, 14580 USA (e-mail: queiroz@wrc.xerox.com).

Publisher Item Identifier S 1057-7149(99)07553-3.

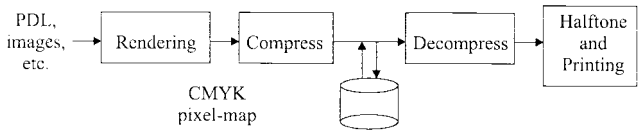

Fig. 1. Image path for generating and printing an image in a high-end printing device (PDL stands for page description languages, e.g., postcript).

printing system path in which a CMYK image bitmap is generated and possibly compressed. JPEG [5] is a standard for image compression and is widely used. Other compressors such as SPIHT [6] are becoming very popular, and work is under way to define a new standard for still-image compression [7]. In this work, we use only JPEG for three basic reasons. First, JPEG is a well-known standard so we assume the readers are well aware of its performance. Second, our tests involve comparisons whose results are not likely to change by replacing the coding mechanism. Last, as a standard, it is the coder in which most readers would actually use the results of this work. We here study color transformation for compression of CMYK. Similar to the way in which RGB images are commonly converted to luminance-chrominance color spaces such as YCbCr before compression, we would like to understand which transformations would be the best to apply to CMYK images for the same purpose. Along with color transformations, we also discuss the applicability of subsampling for *chrominance* planes.

II. Device Space and Distortion Measure

A compression mechanism must be evaluated through its rate-distortion (RD) tradeoff so we need to define a distortion measure. In color management, CIE's ΔE^*_{ab} [8], [9] is a common error measure for color patches. (We use the notation ΔE as a shorthand to ΔE^*_{ab}.) For natural images the spatial-CIELAB difference metric has been proposed [10], in which linear filtering is applied to luminance-chrominance color planes and then CIE ΔE^*_{ab} is computed on a pixel-by-pixel basis forming an *error* image. We propose a practical simplified variation of [10] and refer to it as $S\Delta E$.

CMYK is generally a device color space. One might be able to invert the UCR strategy and obtain RGB values, but they still would be device-space RGB values. Those values have little meaning until they are translated into a standard (reference) space. CIELAB is one possible space. Inversion is possible if the image's ICC profile [11] or the printer model (for the device for which the CMYK values were derived) is available. Several devices, including xerographic and nonxerographic printers, are considered. Hence, different CMYK images in this work were created from the same image by submitting the input image (in for example CIELAB) through the device's own color correction LUT. Thus, each device is associated to one printer model LUT (CMYK to CIELAB or to RGB) and to one color correction LUT (CIELAB to CMYK), which are hopefully the inverse of each other and can be inferred from the device's ICC profile. For the printer model and color correction tables used in this paper, the conversion between CIELAB and CMYK, back and forth, yields average ΔE below 2.7 for all images and devices.

The distortion measure $(S\Delta E)$ between two CMYK images used in this paper is performed in a standard color space and is obtained as in Fig. 2. Each image is mapped to Xerox RGB (D50) from CMYK through its corresponding printer model LUT. RGB values are converted to YCbCr through the popular linear transformation from [5]. Next, each luminance channel is filtered with an 11×11 filter $h_L(m,n)$, while each chrominance channel is filtered with an 11×11 filter $h_C(m,n)$. The resulting filtered images are converted

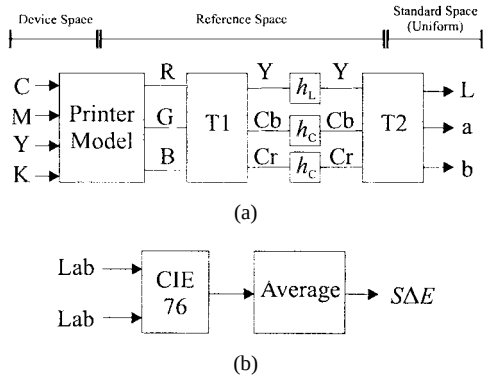

Fig. 2. Computation of $S\Delta E$. (a) Computation of filtered CIELAB images. (b) Error measure from comparing two CIELAB images. T1 and T2 are color transformations, while h_L and h_C are HVS-derived linear filters.

to CIELAB from which $\Delta E(m,n)$ (CIE 76) is measured for every pixel (m,n). $S\Delta E$ is taken simply as the average of the $\Delta E(m,n)$.

The proposed measure is simply the average error in a perceptually uniform color space, with the only difference being that the images are prefiltered to remove "invisible" noise, which is the idea of spatial-CIELAB [10]. We however want to keep the filtering process as simple as possible because of the large number of measurements. In order to better remove invisible error patterns, one may try to approximate the human visual system (HVS), whose transfer function is complex and nonlinear. Linear transfer function approximations of the HVS have been attempted by several researchers by analyzing the sensitivity of observers to sinusoidal gratings [12]–[16]. Studies to better comprehend the human sensitivity to chrominance signals are still under way. In reality the one-dimensional (1-D) transfer function of the HVS is a multidimensional function, depending on 1) location in the gamut, 2) change direction in the gamut, and 3) frequency and amplitude of the change. In our simplification efforts we employ some ad-hoc restrictions: a separable model, filter size (support) of 11×11, and linear-phase (symmetric) filters. The filters used for luminance and chrominance were derived from known HVS transfer curves which were mapped to simpler functions. The luminance model was chosen as [13]

$$H(f) = 2.46(0.1 + 0.25f)e^{-0.25f} \tag{1}$$

where f is given in number of cycles per degree (cpd) of visual angle subtended and where the peak occurs at 3.75 cpd. The chrominance curve is simply

$$H(f) = e^{-0.205f}. \tag{2}$$

It is necessary to determine the maximum visible frequency which is a function of resolution and viewer distance from the image. As a reference we have chosen a resolution of 300 pixels per inch (ppi) and a distance of 12 in from the image. By least squares finite impulse response (FIR) design of separable filters we found approximation filters for luminance $(h_L(m,n))$ and chrominance $(h_C(m,n))$ which are given in Table I. Not only are shorter filters faster to compute, but they also avoid the artificial periodic extension implied when filtering is performed in the discrete Fourier transform (DFT) domain. Long periodic filters with very poor spatial resolution, often produce localized artifacts. In other words we trade poorer frequency selectivity for better space localization.

In any case, the goal of filtering is merely to remove low-visibility noise which interfere with MSE-type error measures. Furthermore, the reader must have in mind that nowhere in this paper is $S\Delta E$ taken as an absolute value, but is used to compare different compression methods. Several of the results in the next sections were also

TABLE I
LUMINANCE (LEFT) AND CHROMINANCE (RIGHT) FILTERS

0	0	1	0	-5	-8	-5	0	1	0	0
0	1	2	-1	-13	-24	-13	-1	2	1	0
1	2	3	-1	-27	-51	-27	-1	3	2	1
0	-1	-1	1	11	21	11	1	-1	-1	0
-5	-13	-27	11	224	418	224	11	-27	-13	-5
-8	-24	-51	21	418	780	418	21	-51	-24	-8
-5	-13	-27	11	224	418	224	11	-27	-13	-5
0	-1	-1	1	11	21	11	1	-1	-1	0
1	2	3	-1	-27	-51	-27	-1	3	2	1
0	1	2	-1	-13	-24	-13	-1	2	1	0
0	0	1	0	-5	-8	-5	0	1	0	0

0	0	0	1	2	3	2	1	0	0	0
0	0	1	4	8	10	8	4	1	0	0
0	1	5	13	28	38	28	13	5	1	0
1	4	13	37	77	103	77	37	13	4	1
2	8	28	77	161	216	161	77	28	8	2
3	10	38	103	216	289	216	103	38	10	3
2	8	28	77	161	216	161	77	28	8	2
1	4	13	37	77	103	77	37	13	4	1
0	1	5	13	28	38	28	13	5	1	0
0	0	1	4	8	10	8	4	1	0	0
0	0	0	1	2	3	2	1	0	0	0

recomputed with variations in filter design and $S\Delta E$ computation. The relative performance of different algorithms was unchanged.

As a comparison, the PSNR between the CMYK images in the native device-CMYK spaces were also computed and will be presented as an alternative error measure.

III. DATA-INDEPENDENT COLOR TRANSFORMATION

Because of the difficulties in converting to and from device-dependent four-dimensional (4-D) color spaces, the CMYK separations are usually compressed independently. In a JPEG framework this translates into compressing four color channels at full resolution. In a recent standard [17], JPEG defined a file format and several color spaces for compression. The options for 4-D color spaces are CMYK, CMY and YCbCrK. CMY is a three-dimensional (3-D) color space where the ink coverage is fixed. YCbCrK derives from CMYK, in which CMY is converted to RGB and from there to YCbCr. In this case, the black channel K remains untouched.

We introduce yet another 4-D device-independent color space. Fig. 3 shows CMYK planes for one of the test images color corrected for the xerographic printer. For most device calibrations, luminance components are heavily built into the K channel. By inverting CMY into RGB and converting to YCbCr, the resulting luminance component Y also contains much of the luminance of the original image. The color channels for YCbCr derived from CMY are also shown in Fig. 3. We propose to also invert K, obtaining a "white" channel ($W = 1 - K$). The W channel is then combined with the luminance of YCbCr. Note that the sharp edges of the luminance channels are also represented in the W channel [Fig. 3(d)]. We propose to try to remove the extra redundancy between the Y and W channels mainly in regard to sharp edges. In our proposal, we produce two output channels from Y and W: one (Y_+) contains the average of Y and W and the other (Y_-) contains the difference between them. We refer to the resulting color space as YYCC, short for Y_+Y_-CbCr. The overall transformation diagram is shown in Fig. 4. Fig. 3(h) and (i) shows the Y_+ and Y_- images, which can be compared to the images W and Y in Fig. 3(d) and (g). Y_+ resembles Y, but the sharp edges in W seem to have been incorporated into Y_+ instead of Y_-. Note in Fig. 3 that Y_- has characteristics of both luminance and chrominance channels and softer edges. This facilitates compression as sharp edges are more concentrated in one channel. In other words, compression in YYCC space demands compression of images in Fig. 3(e), (f), (h), and (i), while compression in YCbCrK space demands compression of images in Fig. 3(d)–(g), and compression of the CMYK channels demands compression of images in Fig. 3(a)–(d).

Another issue in the compression of color images is the subsampling factor for each color plane. It is a common practice to subsample chrominance signals in a YCbCr color space by a factor of two in each direction. Similar benefits are expected by subsampling Cb and Cr in both YCbCrK and YYCC color spaces. In reality, even monochrome images can benefit from subsampling. It is known that for higher compression ratios it is preferred to subsample the image first and then apply higher quality JPEG compression [18], than to simply compress the image with lower quality factor. The same is true for every color channel. What we need to understand is where the breakpoint lies. We will show that in a 4-D color space there is no need to subsample the chrominance channels, except for very high compression ratios where the overall quality is compromised.

The color transformations to YCbCrK and YYCC are said to be data-independent because they are not dependent on the image contents. Other methods such as those based on the KLT devise the transformation after computing the input image statistics [19] with the goal of decorrelating the input color planes.

IV. COMPARATIVE EVALUATION

For comparison, each method is evaluated through an RD curve plot, employing baseline JPEG. In all tests, to maintain a common reference, only the example (default) quantizer and Huffman tables were used and the curves were obtained by scaling the quantizer tables by a common multiplicative ("quality") factor. The CMYK channels as well as the luminance in YCbCrK and the transformed luminance channels in YYCC were subject to JPEG's default luminance table, while channels Cb and Cr were subject to the default chrominance tables.

Tests were performed for several printers and images. As discussed, each printer is associated to its own color correction and printer model tables, so that for each printer a different set of CMYK values is generated. A number of transform/compression configurations were tested: CMYK, YYCC with and without chrominance subsampling, YCbCrK with and without chrominance subsampling, KLT-based using luminance table for all channels, and KLT-based using both luminance and chrominance tables. Distortion was computed as both SΔE and peak signal-to-noise ratio (PSNR) between the CMYK data. For conciseness, only few representative results are presented in condensed form.

In Fig. 5, we show the RD plots comparing CMYK, YYCC, and YCbCrK averaged for all images, with and without subsampling chrominance planes. Note that subsampling the chrominance is only advantageous for very low bit-rates. The breakpoint for subsampling occurs at rates generally below 0.2 b/pel (compression ratio larger than 160 : 1). Also, YYCC consistently outperforms the others in terms of SΔE and PSNR.

The reason for the great advantage of YYCC is the softening of edges in W, which has large contrast. Therefore, in situations where this scenario does not occur one may expect less or no advantage

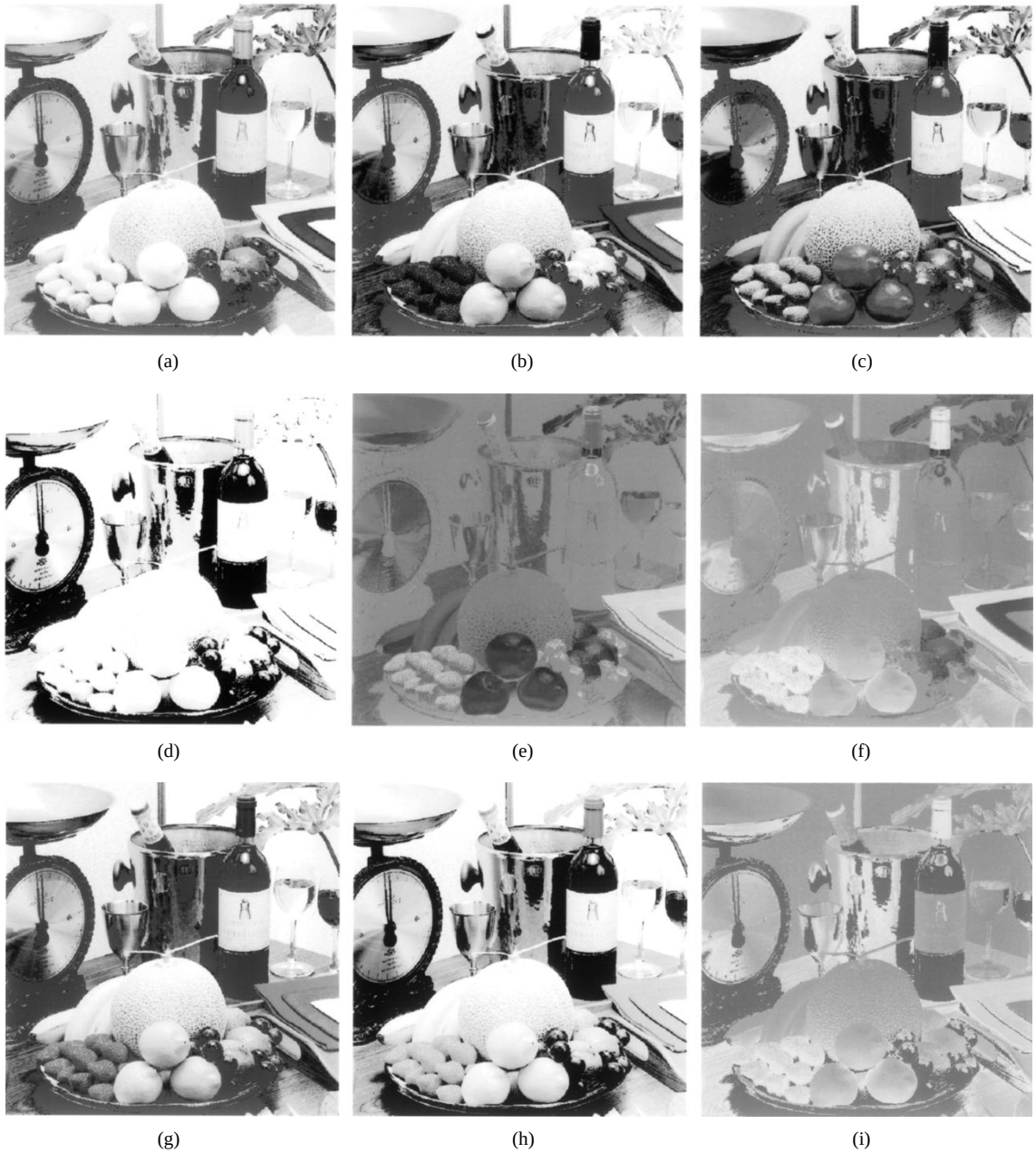

(a) (b) (c)

(d) (e) (f)

(g) (h) (i)

Fig. 3. Color planes of the reference image. (a) Inverse cyan. (b) Inverse magenta. (c) Inverse yellow. (d) Inverse black or "white" (W). Images (e)–(g) correspond to YCbCr channels obtained from transforming images (a)–(c). (e) Cb. (f) Cr. (g) Y. (h) $Y_+ = \frac{1}{2}(Y+W)$. (i) $Y_- = \frac{1}{2}(Y-W)$.

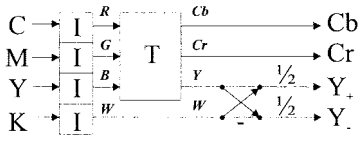

Fig. 4. Computation of YYCC. "I" means inversion and T is an RGB-YCbCr transformation.

in using YYCC. The lower the correlation between Y and W, the smaller the advantage. Another experiment was made by devising CMY data for monitors and dye-sublimation printers while using a fixed UCR strategy (80%) to find K. This would result in having K (and W) with less contrast and much more noise. The averaged results for several images and for the two devices are shown in Fig. 6(a). Note the unimpressive performance of the YYCC space because of the decorrelation between Y and W (K). The plots in Fig. 5 were averaged over several images, which masks some individual but interesting results. For example, for one of the test images whose results are shown in Fig. 6(b), the performance of CMYK independent compression is substantially better than the others for low compression ratios. This particular test image is scanned printed material and still has strong halftone artifacts. The more noise the lower the correlation among color planes. Tests were repeated for two other images of similar nature and the results are consistent with that of Fig. 6, i.e., there is a breakpoint in compression ratio after which it is advantageous not to transform the image.

Fig. 7 shows a comparison of compression in YYCC and CMYK color spaces against image-dependent KLT-based transformations. The KLT-based method is presumed to be optimal in the sense of decorrelating the color planes. However, it does not affect the spatial correlations and there is still the factor of matching the color transformation to the compression scheme. Fig. 7 shows average

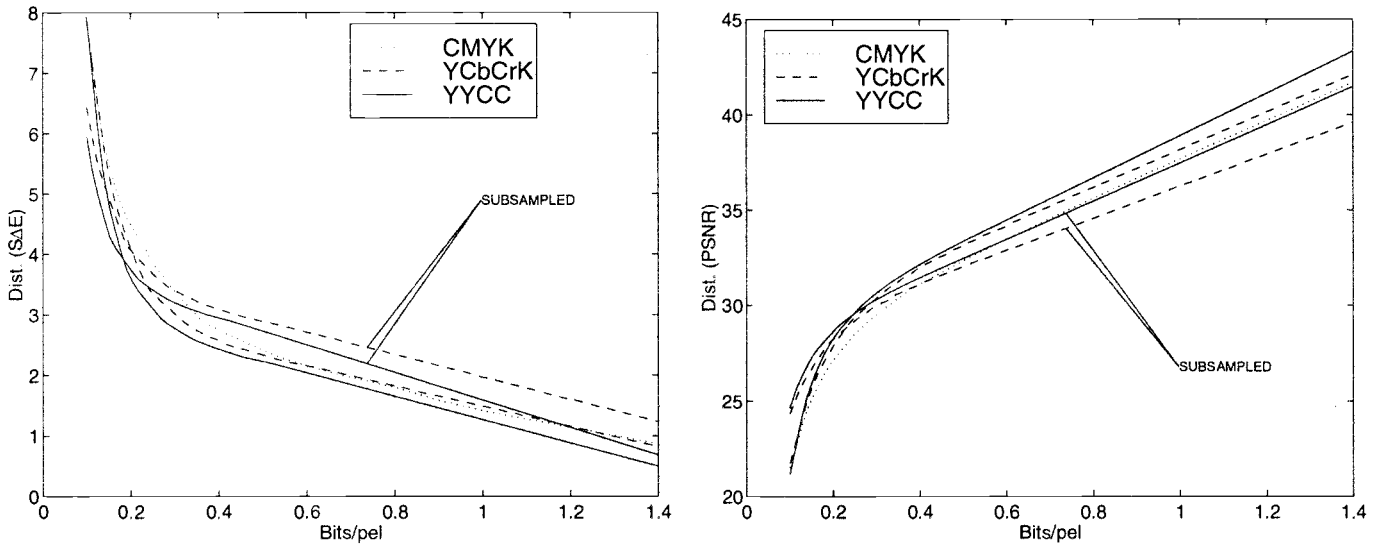

Fig. 5. RD plots comparing CMYK, YCbCrK and YYCC averaged over several images for a xerographic printer. Tests were made with and without chrominance subsampling.

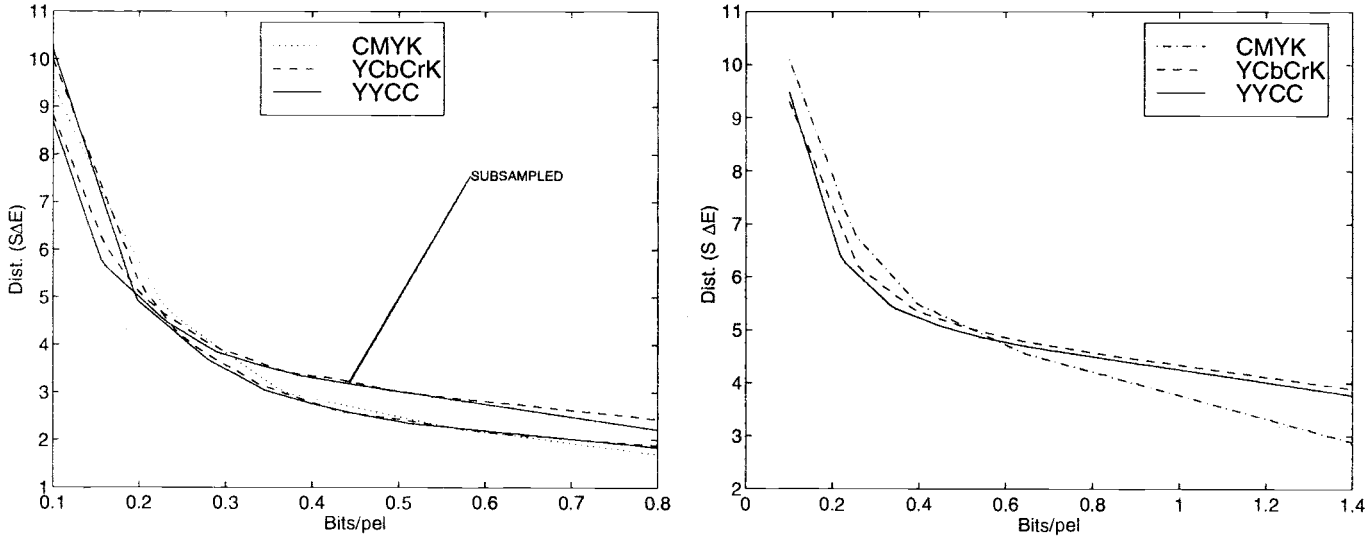

(a) (b)

Fig. 6. RD plots for situations where there is little or no advantage in converting the image to YYCC. (a) Fixed UCR strategy for several device spaces and images. (b) Noisy scanned image for the xerographic device.

RD plots for all images, for the xerographic printer, and using both SΔE and PSNR as distortion measures. The two KLT plots represent two different compression schemes. In the first, all KLT-resulting planes were subject to luminance quantizer tables in JPEG. In the second case, the two color planes with the higher energy were subject to luminance quantizer tables while the other two were subject to chrominance quantizer tables. The results in Fig. 7 indicate that the performance of YYCC comes very close to the image-adapted expensive KLT-method which is presumed to be statistically optimal.

The reader is encouraged to reproduce the experiments in this correspondence. All steps in the transformation to YYCC and in the computation of SΔE are straighforward, mostly linear and invertible. Just the color correction to obtain the CMYK values and the printer model are printer dependent. Such tables can be derived, for example, from the printer's ICC profile.

V. Conclusions

The data supports the following preliminary conclusions for the devices tested.

1) YYCC consistently outperforms YCbCrK.
2) The higher the noise in the color planes the lower the correlation among planes and the smaller the advantage of color transformation.
3) For low compression of noisy halftoned images it is better to compress CMYK independently.
4) Chrominance subsampling is not desired for most bit-rates of interest.
5) The best of YYCC and CMYK is only slightly inferior to KLT transformations.

Based on the preliminary conclusions, the main conclusion of this work is that CMYK images can be efficiently compressed using

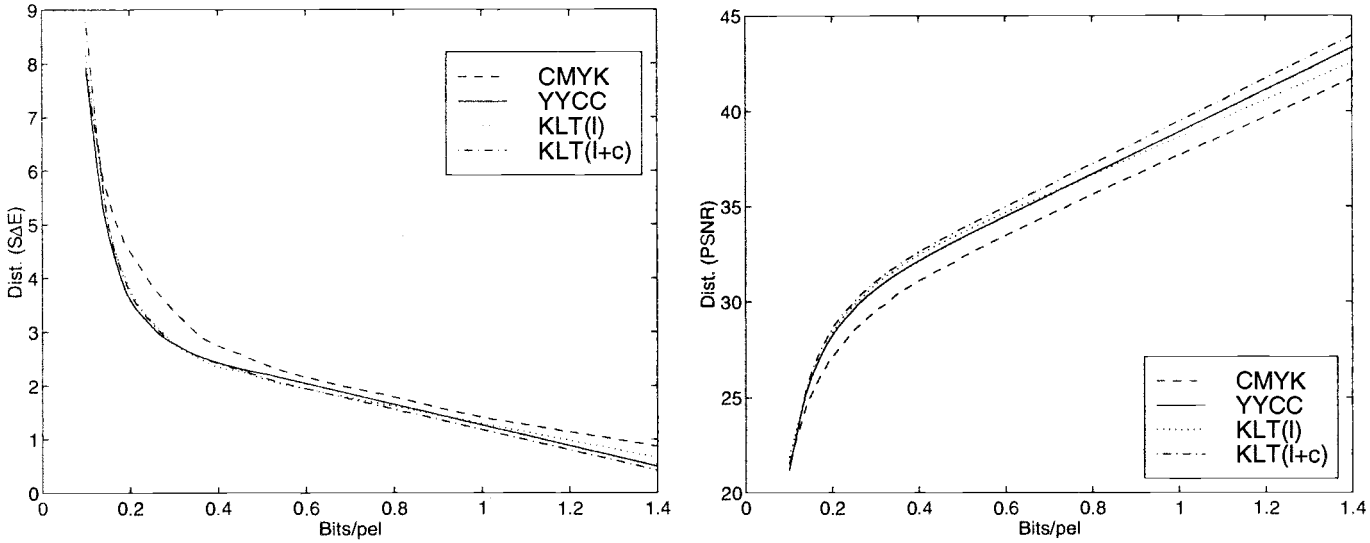

Fig. 7. RD plots comparing CMYK, YYCC, and the KLT for a xerographic printer. Results are averaged for all images. The two KLT types correspond to use only the luminance table for all transformed planes, or both luminance and chrominance tables (two planes for each).

a YYCC color space (without chrominance subsampling), with the notable exception of low-ratio compression of very active (or noisy) images, which may be compressed in their native CMYK color space.

REFERENCES

[1] G. Sharma and H. J. Trussell, "Digital color imaging," *IEEE Trans. Image Processing*, vol. 6, pp. 901–932, July 1997.
[2] R. W. G. Hunt, *The Reproduction of Color*, 3rd ed. New York: Wiley, 1975.
[3] H. R. Kang, *Color Technology for Electronic Imaging Devices*. SPIEs, 1997.
[4] E. Giorgianni, T. Madden, *Digital Color Management: Encoding Solutions*. Reading, MA: Addison-Wesley, 1998.
[5] W. B. Pennebaker and J. L. Mitchell, *JPEG: Still Image Compression Standard*. New York: Van Nostrand Reinhold, 1993.
[6] A. Said and W. A. Pearlman, "A new fast and efficient image codec based on set partitioning in hierarchical trees," *IEEE Trans. Circuits Syst. Video Technol.*, vol. 6, pp. 243–250, June 1996.
[7] Call for contributions for JPEG 2000, ISO/IEC, JTC1/SC29/WG1, N505, Mar. 21, 1997.
[8] *Colorimetry*, CIE publ. no. 15.2, Bur. Centr. CIE, Vienna, Austria, 1986.
[9] A. R. Robertson, "Historical development of CIE recommended color difference equations," *Color Res. Appl.*, vol. 15, pp. 167–170, June 1990.
[10] X. M. Zhang and B. A. Wandell, "A spatial extension to CIELAB for digital color image reproduction," in *Proc. Soc. Information Display Symp.*, 1996.
[11] *ICC Profile Format Specification*, Int. Color Consort., Ver. 3.4, Aug. 15, 1997.
[12] J. L. Mannos and D. J. Sakrison, "The effect of visual fidelity criterion on the encoding of images," *IEEE Trans. Inform. Theory*, vol. IT-20, pp. 525–536, July 1974.
[13] B. Chitpraset and K. R. Rao, "Human visual weighted progressive image transmission," *IEEE Trans. Commun.*, vol. 38, pp. 1040–1044, July 1990.
[14] D. H. Kelly, "Spatial and temporal interactions in color vision," *J. Imag. Technol.*, vol. 15, pp. 82–89, Apr. 1989.
[15] K. T. Mullen, "The contrast sensitivity of human color vision to red-green and blue-yellow chromatic gratings," *J. Physiol.*, vol. 359, pp. 381–400, 1985.
[16] S. L. Guth, "The chromatic contrast sensitivity myth," in *Proc. 5th Color Imaging Conf.*, Scottsdale, AZ, 1997, pp. 23–26.
[17] ISO/IEC CD 10918-3, Info. Technology—Digital compression and coding of continuous tone still images—Part 3: Extensions, Nov. 13, 1994.
[18] B. Zeng and A. Venetsanopoulos, "A JPEG-based interpolative coding scheme," *Proc. Int. Conf. Acoust., Speech, Signal Processing*, Minneapolis, MN, 1993, vol. V, pp. 393–396.
[19] P. De Neve, W. Philips, K. Denecker, and I. Lemahieu, "Introducing a decorrelated color space in the lossy compression of pre-press applications," in *Proc. 5th Color Imaging Conf.*, Scottsdale, AZ, 1997, pp. 88–92.

Semi-Fixed-Length Motion Vector Coding for H.263-Based Low Bit Rate Video Compression

Guy Côté, Michael Gallant, and Faouzi Kossentini

***Abstract*—We present a semi-fixed-length motion vector coding method for H.263-based low bit rate video compression. The method exploits structural constraints within the motion field. The motion vectors are encoded using semi-fixed-length codes, yielding essentially the same levels of rate-distortion performance and subjective quality achieved by H.263's Huffman-based variable length codes in a noiseless environment. However, such codes provide substantially higher error resilience in a noisy environment.**

***Index Terms*—Error resilience, H.263, video coding, video compression.**

I. INTRODUCTION

Low bit rate video compression is becoming increasingly important due to present and forthcoming video applications, such as video telephony over analog telephone lines or over wireless channels. This

Manuscript received April 2, 1998; revised August 18, 1998. This work was supported by the Natural Sciences and Engineering Research Council of Canada. The associate editor coordinating the review of this manuscript and approving it for publication was Dr. Antonio Ortega.

The authors are with the Department of Electrical and Computer Engineering, University of British Columbia, Vancouver, B.C. V6T 1Z4, Canada (e-mail: faouzi@ee.ubc.ca).

Publisher Item Identifier S 1057-7149(99)07561-2.